NUMERICAL SIMULATION OF SOLITARY SURFACE WAVES IN A DISCRETE MODEL OF AN INCOMPRESSIBLE LIQUID

A. M. Frank

UDC 532.59

Solitary surface waves are usually studied theoretically in the framework of the shallow-water model. Solitary waves have also been studied on the basis of a numerical solution of the Navier–Stokes equations [1], as well as the Cauchy–Poisson problem [2].

In the present paper we consider the numerical simulation of solitary waves on the basis of a discrete model of an incompressible liquid. The essence of the approach is the modeling of an incompressible continuum with the help of a finite system of particles with holonomic constraints [3]. Even when the spatial quantization is large, this model is consistent in the sense of the fundamental conservation laws of mechanics. The discrete model considered here is constructed with the help of a regular quadrangular grid and, therefore, is somewhat similar to the Lagrangian method LINC [4]. A similar discrete model was used in [5, 6]. We present calculated results for solitary waves of various amplitudes, the kinematic and dynamic characteristics of the run-up of solitary waves on vertical and inclined walls, and also a comparison between the available theoretical and experimental results.

1. Description of the Model. We consider a layer of incompressible liquid with a free surface and a finite depth. We split up the volume Ω occupied by the liquid into quadrangles (Fig. 1). We assume that at the grid points there are particles, where the mass of a particle is the average of the masses of the quadrangles corresponding to the given grid point. For example, for internal grid points $m_{i,j} = (\rho/4)(V_{i,j} + V_{i-1,j} + V_{i-1,j-1} + V_{i,j-1})$ (ρ is the density of the liquid). Hence the continuous medium is approximated by a finite system of particles. It is well known that in the continuum model of an incompressible liquid there are no potential interactions between the particles of the medium (i.e., no internal energy). In addition, the nature of the forces of interaction are not in general considered. Instead, the kinematic condition of incompressibility is introduced, which is a restriction on the possible motion of the medium. In our discrete model it is also necessary to introduce a discrete incompressibility condition, guaranteeing the constancy of the volume of liquid. Such a condition could be the requirement that the areas of all quadrangles are constant ($V_{i,j}$ = const) during the motion of the medium. The area of each quadrangle is a function of the coordinates of its corners $V_{i,j} = V(\mathbf{r}_{i,j}, \mathbf{r}_{i,j+1}, \mathbf{r}_{i+1,j+1}, \mathbf{r}_{i+1,j})$; therefore, the relation $V_{i,j}$ = const represents a set of holonomic constraints imposed on the motion of the particles. For particles lying on the solid boundaries we impose the additional restriction that motion is possible only along the boundary and that the particles cannot penetrate the boundary. These restrictions are also obviously holonomic constraints. For example, for particles lying on the right wall the constraint has the form $y_{i,j} - y^0 - (x_{i,j} - x^0)\tan\alpha = 0$.

Therefore, we obtain a finite mechanical system with holonomic constraints as a model of the incompressible liquid. The force of gravity must be introduced in order to describe wave motion. The simplest method of doing this [4-6] is to assume that the force of gravity $m_{i,j}\mathbf{g}$ acts on each particle. However, it is easily shown in this case that when the volume Ω is broken up with the help of a nonorthogonal grid there are situations in which the unperturbed layer of liquid does not have minimum potential energy and, therefore, the equilibrium

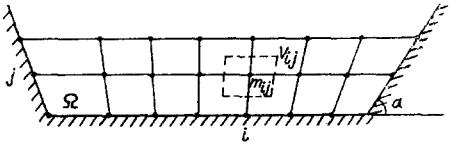

Fig. 1

Krasnoyarsk. Translated from Zhurnal Prikladnoi Mekhaniki i Tekhnicheskoi Fiziki, No. 3, pp. 95-101, May-June, 1989. Original article submitted January 28, 1988.

0021-8944/89/3003-0431$12.50

position is unstable. This leads to unphysical motion of the particles in the calculations and, as a result, to the breakdown of the solution. Therefore, the force of gravity is introduced differently in our treatment. The potential energy of the layer of liquid is $\rho g \int_{\Omega} y\,dx\,dy$. The discrete medium occupies a region Ω' with a free boundary given by the broken line formed by the surface particles. We assume that the potential energy of our discrete system is $\Pi = \rho g \int_{\Omega'} y\,dx\,dy$. Then Π is a minimum, subject to the condition of a constant area Ω', when the free surface is horizontal. It is also evident that Π depends only on the coordinates of the surface particles. The Lagrangian of the discrete system then has the form

$$L = \frac{1}{2}\sum_{i,j} m_{i,j}(\dot{\mathbf{r}}_{i,j})^2 - \Pi. \tag{1.1}$$

To derive the equations of motion, (1.1) must be supplemented by the holonomic constraints corresponding to the incompressibility condition

$$V_{i,j} = \text{const} \tag{1.2}$$

and the nonpenetrability condition

$$\gamma_{p,q}(t, \mathbf{r}_{i,j}) = 0. \tag{1.3}$$

In (1.3) the time t appears explicitly in the case when one of the solid boundaries moves according to a prescribed equation. For example, putting $\alpha = \alpha(t)$, we can obtain an oscillating right wall; a type of wave generator. The constrains (1.2) and (1.3) are written in the general form

$$f_s(t, \mathbf{r}) = 0, \tag{1.4}$$

where s = (i, j) is a multiple index specifying the number of the constraint; r is a vector composed of the coordinates of all particles. The equations of motion of our discrete system can now be found from Hamilton's principle using the technique of Lagrange multipliers [7, 3]:

$$m_k\dot{\mathbf{u}}_k = \sum_s \lambda_s \frac{\partial f_s}{\partial \mathbf{r}_k} - \frac{\partial \Pi}{\partial \mathbf{r}_k}, \quad \dot{\mathbf{r}}_k = \mathbf{u}_k, \; f_s(t, \mathbf{r}) = 0. \tag{1.5}$$

Here k = (i, j) is a multiple index specifying the number of particle; $\mathbf{u}_k$ is the velocity of particle k, $\partial f_s/\partial \mathbf{r}_k = (\partial f_s/\partial x_k, \partial f_s/\partial y_k)$; λ_s is a Lagrange multiplier. We note that, regardless of the number of degrees of freedom, system (1.5) contains the fundamental conservation laws of mechanics. For example, if the constraints do not depend explicitly on t, then the total energy of the system is conserved. If the boundary constraints (1.3) are removed and g = 0, then the momentum and angular momentum of the system are conserved. The conservation laws follow from the invariance of the internal constraints (1.2), and hence also the total Lagrangian, to the corresponding displacement and rotation groups.

A special algorithm was worked out for the numerical solution of (1.5), which for g = 0 is completely conservative, i.e., the method ensures that the above conservation laws hold for any value of the time stepsize τ. When $g \neq 0$, the energy is conserved to order τ^2 and, in practice, it varies by no more than a few tenths of a percent. The algorithm has been described in detail in [8]; here we present only the basic computational formulas:

$$\begin{gathered}
\mathbf{r}_k^{n+1/2} = \mathbf{r}_k^n + \frac{\tau}{2}\mathbf{u}_k^n, \\
m_k\mathbf{u}_k^{n+1} = m_k\mathbf{u}_k^n + \tau\sum_s \lambda_s \mathbf{G}_{sk} - \tau\frac{\partial \Pi}{\partial \mathbf{r}_k}(\mathbf{r}^{n+1/2}), \\
\mathbf{u}_k^{n+1/2} = \frac{1}{2}(\mathbf{u}_k^{n+1} + \mathbf{u}_k^n), \; \mathbf{r}_k^{n+1} = \mathbf{r}_k^n + \tau\mathbf{u}_k^{n+1/2}, \; \sum_s A_{sp}\lambda_s = F_p,
\end{gathered} \tag{1.6}$$

where $\mathbf{G}_{sk} = \dfrac{\partial f_s}{\partial \mathbf{r}_k}(t_{n+1/2}, \mathbf{r}^{n+1/2})$; $A_{sp} = \sum_k \dfrac{1}{m_k}\mathbf{G}_{sk}\cdot\mathbf{G}_{pk}$; $F_p = -\dfrac{2}{\tau}\sum_k \mathbf{G}_{pk}\cdot\left[\mathbf{u}_k^n - \dfrac{\tau}{2m_k}\dfrac{\partial \Pi}{\partial \mathbf{r}_k}(\mathbf{r}^{n+1/2})\right]$.

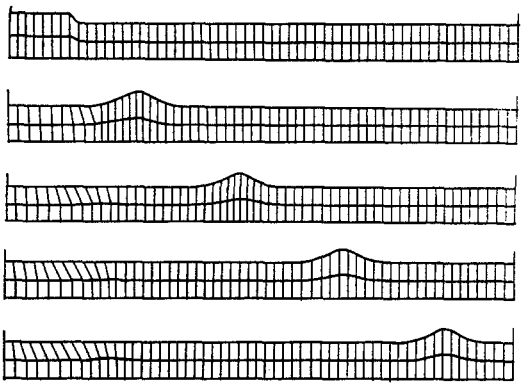

Fig. 2

TABLE 1

A	$\sqrt{1+A}$	c
0,52	1,233	1,231
0,41	1,187	1,185
0,29	1,136	1,134
0,195	1,093	1,089

We note that on each time step it is required to solve a system of linear equations, where the matrix A of these equations is symmetric and positive definite. Also, many of its elements are zero, since the vectors $\mathbf{G}_{sk}$ are nonzero only for certain neighboring values of the indices s and k. The method of successive upper relaxation was used to solve the linear system of equations. It was shown in [8] that the algorithm (1.6) ensures that the constraints (1.4) are satisfied to within terms of order τ^2. The stepsize τ is usually chosen from the requirement that (1.4) be satisfied to within a specified accuracy.

The boundary conditions on the solid surfaces, formulated as holonomic constraints (1.3), can be included naturally in the general scheme (1.5) and (1.6). The Lagrange multipliers corresponding to these constraints represent the reaction forces of the walls on the boundary particles and can then be used to compute the forces acting on the walls. In some cases it is more convenient to decrease the dimension of the matrix of the linear system in (1.6) by solving some of the boundary constraints (1.3) explicitly, thereby reducing the number of relevant degrees of freedom. For example, in the calculations discussed below, only the x coordinates of the particles on the flat bottom were treated as unknowns. In other words, only the x coordinates of these particles were included as generalized coordinates of the entire system. Besides reducing the dimension of the system of equations, this device also leads to zero second components for some of the vectors $\mathbf{G}_{sk}$ (corresponding to derivatives of the volume near the boundary with respect to the coordinates of the boundary particles).

2. Formulation of the Problem. Results of Calculations. The first problem is to obtain numerical solutions of the solitary wave type. We considered a layer of liquid in a trough with a horizontal bottom and vertical lateral walls with depth H = 1 and length L = 58. The density of the liquid $\rho = 1$ and the gravitational acceleration $g = 1$. These variables correspond to transformation of the original equations to dimensionless form with the help of the following natural units of measurement: ρ, H, $U_* = \sqrt{gH}$, $T_* = H/U$. The coordinate system was chosen such that $y = 0$ corresponds to the unperturbed free surface and $x = 0$ corresponds to the right wall. The waves were generated at the left end of the trough by creating a local rise in the surface of the liquid (Fig. 2) and the following vertical motion to the first eight surface particles (analogous to a horizontal plate moving downward):

$$v = \begin{cases} -\frac{\pi h}{2T}\sin\left(\frac{\pi t}{T}\right), & 0 \leqslant t \leqslant T, \\ 0, & t > T. \end{cases}$$

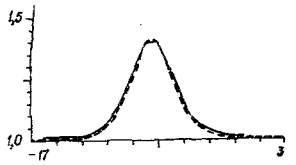

Fig. 3

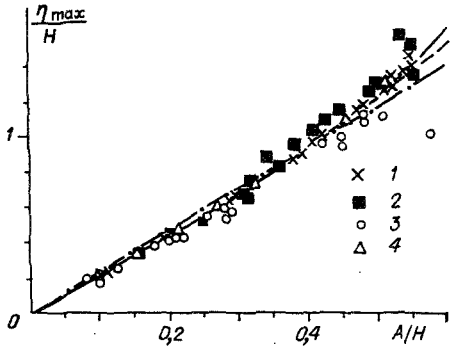

Fig. 4

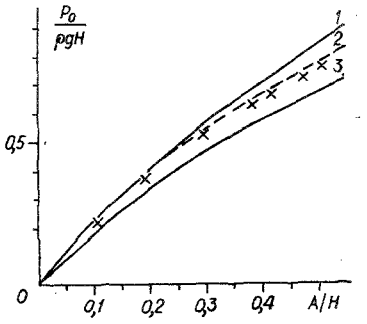

Fig. 5

Here h determines the amplitude of the generated wave and it is possible to choose T such that one can almost completely get rid of the dispersion tail. To suppress strong residual deformations of the grid near the wave generator after the departure of the wave, we introduced an artificial viscoelastic interation in (1.5) for particles near the wave generator. These forces were tuned to the grid such that they had practically no effect on the characteristics of the generated wave or on its propagation. After generation, the wave propagates along the trough and after a certain time its amplitude and shape become established. Figure 3 shows the calculated waveform at the end of the trough with amplitude A = 0.41. The calculation was performed on the grid shown in Fig. 2 with $h_1 = 1$ for the horizontal dimension of a cell, $h_2 = 0.5$ for the vertical dimension, and $\tau = 0.5$ was the time stepsize. The dashed curve shows the waveform obtained from the solution of the shallow-water theory in the second approximation [9].

We also compared the propagation velocity c of the waves with the second approximation of the shallow-water theory. The results are given in Table 1 for several values of the amplitude. We see that even for large spatial quantization our model has the capability of closely reproducing the parameters of solitary waves.

We next considered the run-up of solitary waves on a vertical wall. We used a shorter trough of length L = 22 and initial data obtained from the solution of the preceding problem and the corresponding wave with its crest at x = −14. Linear interpolation of the initial data was used for calculations on the smaller-scale grids. The maximum rise η_{max} on the wall as a function of the amplitude A of the incident wave is shown in Fig. 4 for different grids (set of points 1). For $A \leq 0.3$ we used grids with $h_1 = 1$, $h_2 = 0.5$ and 0.25. For large A the results are given for $h_2 = 0.25$ and 0.125, $h_1 = 1$ and $1 - 0.5$, where the grid was compressed near the right wall. Here we also show the results of laboratory experiments [1, 11] (sets of points 2 and 3) and [10, 12] (dot–dashed and dashed curves) and the calculated results by the SUMMAC method [1] (solid curve) and the spectral method [2] (set of points 4). Note the good agreement between the calculations with the discrete model and the calculations of [1, 2]. The experimental values of the maximum rise have a considerable scatter, but are closer to the calculated results of [12]. Furthermore, we note that for $A < 0.5$ all of the results more or less fall on a single curve, but for $A > 0.5$ a scatter of up to 5% is observed between the calculations on the different grids. The scatter of the experimental data also strongly increases when $A > 0.5$. The sharp, almost threshold nature of this phenomenon suggests that the runup process becomes unstable for waves with amplitude $A \gtrsim 0.5$.

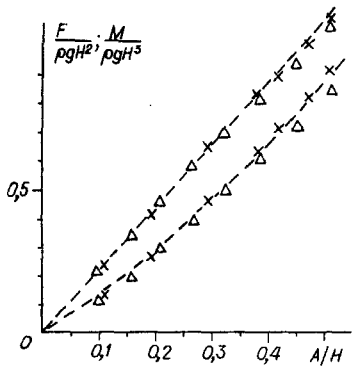

Fig. 6

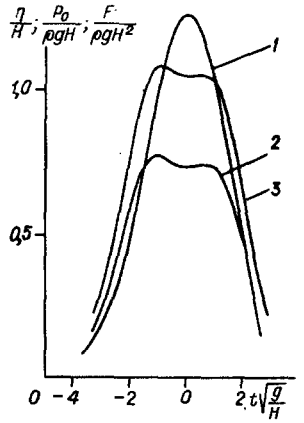

Fig. 7

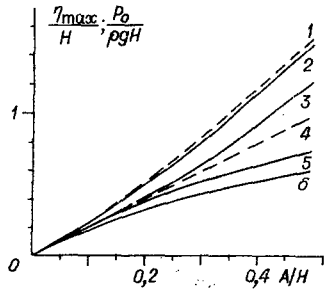

Fig. 8

TABLE 2

tan α				
1			0,5	
A	η_{max}	P_0	η_{max}	P_0
0,113	0,24	0,22	0,27	0,21
0,195	0,44	0,36	0,49	0,32
0,29	0,7	0,49	0,79	0,43
0,41	1,03	0,62	1,17	0,54
0,5	1,3	0,7	1,49	0,61

We also determined the dynamic effect of the waves on the wall. In Fig. 5 the crosses show the calculated maximum value of the pressure on the wall at y = 0 as a function of wave amplitude and in Fig. 6 the crosses show the wave components of the force and torque on the wall, also as functions of wave amplitude. The experimental and calculated data from the papers cited above are also shown, as well as the calculated data from the nonlinear dispersion model of [13] (in Fig. 5 curves 1-3 correspond to [12, 13, 11]; in Fig. 6 the triangles correspond to [2], and the dashed curve to [13]). It is interesting to note that for the calculations in the discrete model with a large grid containing only two cells in the vertical direction, the rise for large-amplitude waves decreases somewhat, while the pressure on the wall increases slightly, such that the results approach those of the calculations in the nonlinear dispersion model [13]. Evidently, as the number of degrees of freedom increases the discrete model goes from a quality of description of the flow typical of simplified hydrodynamic models to a complete description of the flow. We plan to study this question in the future from the point of view of the dispersion relations.

Figure 7 shows the time dependence of the rise η, the pressure P_0 on the wall at y = 0, and the total force (curves 1-3) during the run-up of a wave with amplitude A = 0.51. The double maximum in the pressure curve for large-amplitude waves, observed experimentally in [11], is clearly seen in Fig. 7, as well as the lag of the peak in the rise relative to the peak in the pressure. The pressure and force were calculated as follows. It can be shown that each Lagrange multiplier λ_s in (1.5), corresponding to an internal constraint (1.2), is the approximate value of the function p + ρgy in cell s (p is the total hydrodynamic pressure). Hence, the pressure in cell s is $p_s = \lambda_s - \rho g y_s$ (y_s is the coordinate of a point in cell s). The force acting on particle k can then be calculated as $\mathbf{F}_k = \sum_s p_s \mathbf{G}_{sk}$. Summing over all particles lying in the wall, we find the resultant force F. To obtain the wave force from F we subtract out its hydrodynamic component $(1/2)\rho g H^2$. The torque on the wall is calculated in a similar way. Several choices for $\bar{y}_s$ were tried. For small-scale grids, all gave nearly identical results. For larger grids the best results were obtained when $\bar{y}_s$ was taken to be the vertical coordinate of the center of mass of cell s. The pressure on the wall at y = 0 was determined by linear interpolation along the verticals of two neighboring cells.

The above results are sufficiently accurate and were obtained on a fairly large grid with $h_1 = 1$, $h_2 = 0.25$, and $\tau = 0.2$. The execution time of a typical run was about 10 min on the SM-4 computer. Satisfactory results (differing by not more than 5% from the above calculations) for the rise, pressure, and force are obtained even for $h_1 = 1$, $h_2 = 0.5$, and $\tau = 0.5$. In this case the execution time was about a minute and a half.

We also calculated the run-up of solitary waves on inclined walls with slope 1 and 0.5. The results for the rise and pressure at $y = 0$ are given in Table 2.

Figure 8 shows for comparison the dependence of η_{max} and P_0 on wave amplitude A for a vertical wall and a wall with $\tan\alpha = 0.5$ ($\alpha \approx 27°$). Here the dashed curves 4 give η_{max} and P_0 for a linear theory of run-up on a vertical wall, curves 3 and 5 give the numerical results for a vertical wall, and curves 2 and 6 give the numerical results for an inclined wall. The dashed curve 1 corresponds to the empirical formula $\eta_{max} = KA^{\beta}$ presented in [14] with constants $K = 3.4$ and $\beta = 1.16$ corresponding to $\tan\alpha = 0.5$. We see that the numerical results agree quite closely with this empirical dependence.

We note that similar discrete models can also be constructed on an arbitrary grid, such as the irregular grid of [15], or in general without the use of a grid [3, 16]. The form of Eqs. (1.5) and the algorithm (1.6) remain unchanged; only the form of the constraints (1.2) and (1.3) change, i.e., the particular interpretation of the incompressibility condition and the boundary conditions.

LITERATURE CITED

1. R. Chan and R. Street, "A computer study of finite-amplitude water waves," J. Comp. Phys., 6, 68 (1970).
2. J. D. Fenton and M. M. Rienecker, "A Fourier method of solving nonlinear water-wave problems: application to solitary-wave interactions," J. Fluid Mech., 118, 411 (1982).
3. A. M. Frank and N. N. Yanenko, "Discrete model of an incompressible liquid," in: Computer Modeling of Problems in Mathematical Physics [in Russian], Presidium of the Academy of Sciences of the USSR, Siberian Branch, Krasnoyarsk (1985).
4. C. W. Hirt, J. L. Cook, and T. D. Butler, "A Lagrangian method for calculating the dynamics of an incompressible fluid with free surface," in: 2nd Int. Coll. on Gas Dynamics of Explosions and Reacting Systems, Trans. Sec. on Numerical Methods in Gas Dynamics, Computing Center, Akad. Nauk SSSR, Moscow, Vol. 2 (1971).
5. V. A. Gasilov, V. M. Goloviznin, et al., "On the numerical simulation of the Rayleigh–Taylor instability in an incompressible liquid," Preprint, Inst. of Applied Math., Akad. Nauk SSSR, No. 70, Moscow (1979).
6. R. A. Volkova, L. V. Kruglyakova, et al., "On the simulation of the Rayleigh–Taylor instability in an incompressible liquid in the three-dimensional formulation," Preprint No. 86, Inst. of Appl. Math., Akad. Nauk SSSR, Moscow (1985).
7. H. Goldstein, Classical Mechanics, Addison-Wesley, Reading, Mass. (1950).
8. A. M. Frank, "Completely conservative numerical algorithm for discrete models of an incompressible liquid," in: Simulation in Mechanics [in Russian], Computing Center, Akad. Nauk SSSR, Siberian Branch, ITAM, 1(18), No. 5 (1987).
9. L. V. Ovsyannikov, "Parameters of cnoidal waves," in: Problems of Mathematics and Mechanics [in Russian], Nauka, Novosibirsk (1983).
10. T. Maxworthy, "Experiments on collisions between solitary waves," J. Fluid Mech., 76, 177 (1976).
11. N. N. Zagryadskaya, S. V. Ivanova, et al., "Effect of long waves on a vertical barrier," Izv. VNIIG, 138, 94 (1980).
12. V. Kh. Davletshin, "Force of solitary waves on vertical buildings," Proc. Conf. on Tsunamis, IAP, Akad. Nauk SSSR, Gorkii (1984).
13. M. I. Zheleznyak, "Effect of long waves on solid vertical barriers," in: Run-up of Tsunamis on Beaches [in Russian], IAP, Akad. Nauk SSSR, Gorkii (1985).
14. G. Pedersen and B. Gjevik, "Run-up of solitary waves," J. Fluid Mech., 135, 283 (1983).
15. V. N. Pautov, A. M. Frank, and I. A. Sharaya, "Method of calculating the motion of an incompressible liquid with a free surface on a Dirichlet grid," Preprint No. 16, Computing Center, Akad. Nauk SSSR, Siberian Branch, Krasnoyarsk (1987).
16. A. M. Frank and V. N. Pautov, "On discrete model of inviscid incompressible fluid," in: Proc. Sci. Math. Seminar on Ship Hydrodynamics, BSHC, Varna (1986).